33RD CONGRESS
OF THE INTERNATIONAL COUNCIL
OF THE AERONAUTICAL SCIENCES
STOCKHOLM, SWEDEN, 4-9 SEPTEMBER, 2022

ICAS 2022 SWEDEN

VISCOUS CORRECTION FOR HIGH ORDER IMMERSED INTERFACE METHOD FOR COMPRESSIBLE TRANSONIC FLOWS

Ligia Paola Velandia Luis[1] & Paulo Celso Greco Junior[2]

[1]University of Sao Paulo
[2]University of Sao Paulo

Abstract

An immersed interface method (IIM) is presented, for the analysis of complex geometries within a two dimensional domain inside a compressible flow. The analysis is based on the assumption of inviscid flow. However characteristics present in viscous flows are add with a viscous correction method. For the time and space integration the methods of Runge Kutta and compact finite difference are used, respectively. Also a filter was applied to stabilize the solution process.
A rapid viscous correction method will be applied to the interaction between the boundary layer and the shock wave on airfoils. The boundary layer thickness ahead the shock modifies the position and magnitude of the shock.
The correction method uses the boundary layer sudden increase in equations in two dimensions using the inviscid flow solution and uses iterative process to converge to a viscous correction solution. The aim of this work is to implement the method and compare the numerical results that are similar to the experimental data available in literature .A comparison with Transonic Small Disturbance results is also carried a out.

Keywords: CFD, Método de interface imersa, correção viscosa, fluxo compressível.

1. INTRODUCTION

The present work describes the viscous correction method for the interaction between the shock wave and the boundary layer. The correction is applied to the solution of an Immersed Interface Method (IIM) code, in an iterative process. A fourth order of accuracy approximation is used, in both time and space using the Runge Kutta method and the compact finite difference method, respectively. An implicit like scheme filter was applied to stabilize and smooth the solution while maintaining the order of precision of the compact scheme. The methodology section of this work summarizes the principle of operation that the IIM uses to get the numerical result that solves the system of Euler equations.

1.1 Relevance

The computational fluid dynamics (CFD) is an important tool for the research development in different areas such as Automotive Engineering, Aeronautical Engineering, Industrial Manufacturing, Civil Engineering, Environmental Engineering, Naval Engineer- ing, etc CHUNG, 2010. It works as a complement to the analytical and the experiments approaches. Computational methods has been used in recent decades with relatively good results. In aerodynamics, the CFD analysis is fundamental for investigations, where it is not feasible to create a physical models or the access to wind tunnel is restricted. The CFD is divided into five subprocesses which are: Geometry Definition, meshing, physics definition, solver and post-processing. In this paper we studied the processes of physics definition and post processing, since in the work that was taken as a basis for the correction of viscosity, creation of geometry and meshing for using two meshes had already been made. Because in a complex geometry it is difficult to adjust a regular mesh to the shape of the geometry, and because there is an interest in applying the method to moving geometries, a Eulerian mesh is used for the fluid along with a Lagrangian mesh for the object immersed in the fluid. This method has the potential

to drastically reduce the computational cost because only one of the meshes moves in each step of time and because the lagrangian and the Euilerian mesh has less quantity. The Lagrangian mesh has fewer nodes than the Eulerian mesh. In the solver step the limit layer equations were solved by calculating partial differential equations with the Runge Kutta method.

1.2 METHODOLOGY

The shock / boundary layer interaction is analyzed with the results obtained from the Euler method, the resulting distribution of lift speeds is obtained on the bearing surface that is necessary to calculate the interaction between the shock wave and the boundary layer with the boundary layer equations. Two-dimensional inviscid flow, in this calculation the displacement thickness of the limit layer is found and that thickness generates an effect equivalent to the limit layer to make a modification to the geometry of the lifting surface to obtain a new inviscid solution.

With the created geometry, a new solution is calculated by Euler's method, obtaining a new velocity distribution for a new geometry. The process is repeated until the solution converges and stops varying until a significant variation in speeds is not seen.

In transonic flows, the laminar region near the leading edge and the transition region are not taken into account because it is very small and there are no significant effects on aerodynamic performance, so all the studies are carried out in the turbulent region, which is where it is greater. separation of the flow of the boundary layer of the profile, as one of the aerodynamic problems is knowing the exact point where the turbulent region begins, this process is assumed from the first mesh point of the profile close to the leading edge.

To carry out the viscous correction procedure, the equations are solved in the boundary layer using a two-dimensional numerical integration method developed by SASMAN AND CRESCI (1966) to analyze the compressible boundary layer.

In a turbulent, stable and two-dimensional compressible boundary layer, the continuity and moment equations are

$$\frac{\partial \rho v}{\partial s} + \frac{\partial \rho w}{\partial n} = 0 \tag{1}$$

$$\rho u \frac{\partial v}{\partial s} + \rho w \frac{\partial v}{\partial n} = \frac{\partial p}{\partial s} + \frac{\partial \tau}{\partial n} \tag{2}$$

Where u and w are the velocity components, s its the streamwise and n is the normal, p is the pressure, τ is the shear stress. The variation of the temperature in the transonic flow of the boundary layer is considered using the equations of the transformation described by Mager.

$$\hat{s} = \int_o^s \left(\frac{T_0}{T_{ref}}\right)\left(\frac{T_e}{T_0}\right)^{\frac{\lambda+1}{2(\lambda-1)}} ds \tag{3}$$

$$\hat{n} = \sqrt{\frac{T_e}{T_0}} \int_o^n \left(\frac{\rho}{\rho_0}\right) dn \tag{4}$$

Where T is the temperature, the subscripts e and o are indications for the boundary layer and the stagnation condition, g for adiabatic growth is equal to 1.0 and $Pr = 0.72$, the reference temperature is a function of the Prandtl number, Pr as follows in the equation

$$\frac{T_{ref}}{T_0} = 0,5g + 0,22\sqrt[3]{Pr} + (0,5 - 0,22\sqrt[3]{Pr})\left(\frac{T_e}{T_0}\right) \tag{5}$$

$$\frac{T}{T_0} = 0,5\frac{T_w}{T_0} + 0,22\sqrt[3]{Pr} + (0,5 - 0,22\sqrt[3]{Pr})\left(\frac{T_e}{T_0}\right) \tag{6}$$

Where the subscript w is the wall condition, H represents the shape factor and the momentum thickness θ, the $\hat{H}$ transformed shape factor and $\hat{\theta}$

$$H = \frac{T_w}{T_o}\left[1 - \frac{\gamma-1}{2}M_e^2\right]\hat{H} + \frac{\gamma-1}{2}M_e^2 \tag{7}$$

$$\theta = \left[\frac{T_e}{T_o}\right]^{\frac{\gamma+1}{2(\gamma-1)}} \hat{\theta} \tag{8}$$

$$H = \frac{\delta^*}{\theta} \tag{9}$$

M_e is the Mach number which is denoted by the following expression:

$$M_e = \frac{v_e}{a_e} = \frac{v_e}{a_0}\frac{a_0}{a_e} = \frac{v_e}{a_0}\sqrt{\frac{T_0}{T_e}} \tag{10}$$

$$v_e = \hat{v_e}\sqrt{\frac{T_e}{T_0}} \tag{11}$$

$$\hat{v_e} = M_e a_0 \tag{12}$$

$$M_\infty = \frac{\sqrt{u^2+v^2}}{a_\infty} \tag{13}$$

Where u and v are the velocity components.
And γ is the specific heat ratio. δ^* is the boundary layer displacement thickness, $\hat{\delta}^*$ is the transformed displacement thickness and is used to thicken the geometry of the profile's support surface

$$\delta^* = (\hat{\theta} + \hat{\delta}^*)\left(\frac{T_o}{T_e}\right)^{\frac{3\gamma-1}{2(\gamma-1)}} - \hat{\theta}\left(\frac{T_o}{T_e}\right)^{\frac{\gamma+1}{2(\gamma-1)}} \tag{14}$$

The transformed displacement thickness and momentum thickness for an adiabatic flow are:

$$\hat{\delta}^* = \int_o^{\hat{\delta}} \left(1 - \frac{\hat{U}}{\hat{U}_e}\right) d\hat{n} \tag{15}$$

$$\hat{\theta} = \int_o^{\hat{\delta}} \frac{\hat{U}}{\hat{U}_e}\left(1 - \frac{\hat{U}}{\hat{U}_e}\right) d\hat{n} \tag{16}$$

In the direction $\hat{s}$ the transformed velocity is

$$\hat{U} = u\left(\frac{T_o}{T_e}\right)^{1/2} \tag{17}$$

The transformed momentum integral and transformed moment-of-momentum equations which using a fourth order Runge-Kutta method may then be solved simultaneously, a

$$\frac{\hat{U}}{\hat{U}_e} = \left(\frac{\hat{n}}{\hat{\gamma}}\right)^{\frac{\hat{H}_i - 1}{2}} \tag{18}$$

$\hat{H}_i$ is the adiabatic shape factor

$$\hat{H}_i = \frac{\hat{\delta}^*}{\hat{\theta}} \tag{19}$$

With the form factor $hat H_i$ and the Mager transformation, the functions of momentum θ and form factor H_i transformed as

$$\frac{d\hat{\theta}}{d\hat{s}} = -\frac{\hat{\theta}}{\hat{v_e}}\frac{d\hat{v_e}}{d\hat{s}}(2 + \hat{H}_i) + \left(\frac{T_0}{T_e}\right)^{0.268}\left(\frac{T_0}{T_e}\right)^{1.268}\frac{\tau_w}{\rho_e \hat{v}_e^2} \tag{20}$$

$$\frac{d\hat{H}_i}{d\hat{s}} = -\frac{1}{2\hat{v_e}}\frac{d\hat{v_e}}{d\hat{s}}(\hat{H}_i + 1) + \frac{\hat{H}_i^2 - 1}{\hat{\theta}}\left(\frac{T_{ref}}{T_e}\right)\frac{\tau_w}{\rho_e \hat{v}_e^2}\left[\hat{H}_i + (\hat{H_i} + 1)\int_0^1 \frac{\tau}{\tau_w} d\left(\frac{\hat{n}}{\hat{\delta}}\right)\right] \tag{21}$$

τ_w is the shear stress at the wall, is the empirical relation by Terevin [**?**]

$$\tau_w = 0.123\rho_e \hat{U}_e^2 \left(\frac{\hat{U}_e\hat{\theta}}{v}\right)^{-0.268} \left(\frac{T_e}{T}\right)^{1.268} e^{-1.561\hat{H}_i} \tag{22}$$

Where v is the kinematic viscosity.
The equation is written using in the limit layer the relation of the Mach number and through the relations

$$\int_0^1 \frac{\tau}{\tau_w} d\left(\frac{\hat{n}}{\hat{\delta}}\right) \approx 0.011 \left(\frac{\hat{H}_i - 1}{\hat{H}_i}\right)^2 \frac{2}{C_f} \tag{23}$$

$$C_f = 0.246 e^{-1.561\hat{H}_i} \left(\frac{T_0}{T_e}\right)^{-1} \left(\frac{T_{ref}}{T_0}\right)^{-1} \left(\frac{\mu_{ref}}{\mu_0}\right)^{0.268} \left(\frac{M_e a_0 \hat{\theta}}{\upsilon_0}\right)^{-0.268} \tag{24}$$

$$\frac{T_0}{T_e} = 1 + \frac{\gamma - 1}{2} M_e^2 \tag{25}$$

The transformed moment thickness equations $\hat{\theta}$ and transformed form factor $\hat{H}_i$ result as follows, where A is

$$\frac{d\hat{\theta}}{d\hat{s}} = 1.268 \left(A - \frac{\hat{\theta}}{M_e}\frac{dM_e}{d\hat{s}}(2 + \hat{H}_i)\right) \tag{26}$$

$$\frac{d\hat{H}_i}{d\hat{s}} = A\frac{\hat{H}_i^2 - 1}{\hat{\theta}} \left(\hat{H}_i + \frac{0.022}{C_f}(\hat{H}_i + 1)\left(\frac{\hat{H}_i - 1}{\hat{H}_i}\right)\right) - \frac{\hat{H}_i(\hat{H}_i - 1)(\hat{H}_i + 1)^2}{2M_e}\frac{dM_e}{d\hat{s}} \tag{27}$$

$$A = 0.123 e^{-1.561\hat{H}_i} \left(\frac{T_0}{T_e}\right)^{-1} \left(\frac{T_{ref}}{T_e}\right)^{-1} \left(\frac{T_{ref}}{T_0}\right)^{-1} \left(\frac{\mu_{ref}}{\mu_0}\right)^{0.268} \left(\frac{M_e a_0}{\upsilon_0}\right) \tag{28}$$

The delta data was calculated in a separate code and then the data was incorporated into the IIM code where they were added to the profile and with the new geometry, the new Mach data of the profile were calculated, with these data the new data is generated of delta to generate the new geometry until the result is iterated, thus obtaining the Cp data with viscosity in the limit layer, to bring them closer to the experimental results.

2. Results

The code for the development of the method was written in the Fortran 90 program and executed using the Intel Fortran compiler. Each profile takes approximately 20 hours to run the base code and less than an hour to run the viscous fix code for each fix applied to bring the code to convergence.
A computer with an Intel(R) Core(TM) i5-8400 2.8 GHz CPU with a physical processor has used; six cores; six threads; an ASUS TeK Computer INC motherboard. PRIME H310M-E, a GeForce GTX 1050 Ti/PCIe/SSE2 GPU running on the Linux Mint TARA operating system.
In this work, tests are carried out on two aerodynamic profiles, both with different Mach numbers and angles of attack, as shown in the table 1.

Table 1 – Cases

Airfoil	Mach	Atack angle
NACA 0012	0.75	1
RAE 2822	0.729	2.31

Some cases showed better results than others.

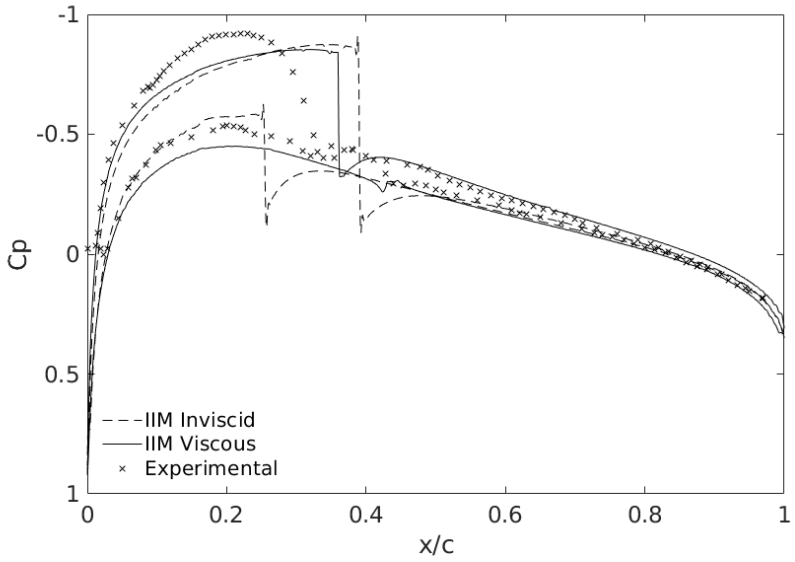

Figure 1 – Pressure coefficient for the NACA 0012 airfoil with M = 0. 750, $\alpha = 1.00^o$, inviscid and without viscous correction.

3. Airfoil section NACA 0012

The viscous correction method was applied to give viscosity effect to an IIM (Immersed Interface Method) code of fourth-order of precision for compressible subsonic flow on the aerodynamic profile NACA 0012. Three cases are presented, which are worked with 1990 nodes in the geometry, 110, nodes in the ns grid, 778 points in the x direction, and 285 in the y direction, 0.0018 the minimum spacing ratio, 0.5542 the $\Delta x_{max}/c$ (maximum spacing in the x direction), 0.2939 the $\Delta y_{max}/c$ (maximum spacing in the x direction) concerning the profile chord. The results are compared with the experimental data of the report AGARD138.

The figures present the pressure coefficient of the inviscid results of the IIM denoted with the dotted line, the Cp data after viscous correction represented with the consecutive line, the experimental data shown with the dotted line in the form of x and finally the data of Cp of the TSD method with applied viscous correction of the work of GRECO2016 which were only incorporated in some cases for verification of the applied viscous correction method.

The graphs of the thickness of the limit litter for each case are also presented, which is represented by the dotted line as the intradorsum and the consecutive line for the thickness in the extradorsum, as well as the graphs of the alteration of the geometry due to the thickness generation δ^* also the pressure field and Mach number fields are presented for all the cases.

3.1 Mach=0.750, $\alpha = 1.00^o$

In this case, it can be seen that the shock wave generated by the profile is highly defined and separates from the chord distance of the experimental results because the Mach number is high. This is caused by the effects of physical phenomena, and the lack of viscosity in the limit layer because Euler's equations do not present viscous terms; Then, when applying the viscosity correction with the limit layer equations, it is observed that the shock wave has an approach to the shock wave in the experimental case, although it continues to show the shock wave defined in the upper surface, although in the lower surface it is smoothed out the wave and approached the experimental pressure coefficient data.

The displacement thickness of the boundary layer 3 increases notably when there is separation of the shock wave, approximately at 45% of the aerodynamic chord of the airfoil in this case; and although it is small compared to the thickness of the original aerodynamic profile, it is not evident how much the thickening of δ^* is even in figure 2. Likewise, viscous effects cause the geometry of the profile to change. The displacement thickness of the boundary layer 3 increases notably when there is separation of the shock wave, approximately at 45% of the aerodynamic chord of the airfoil in this

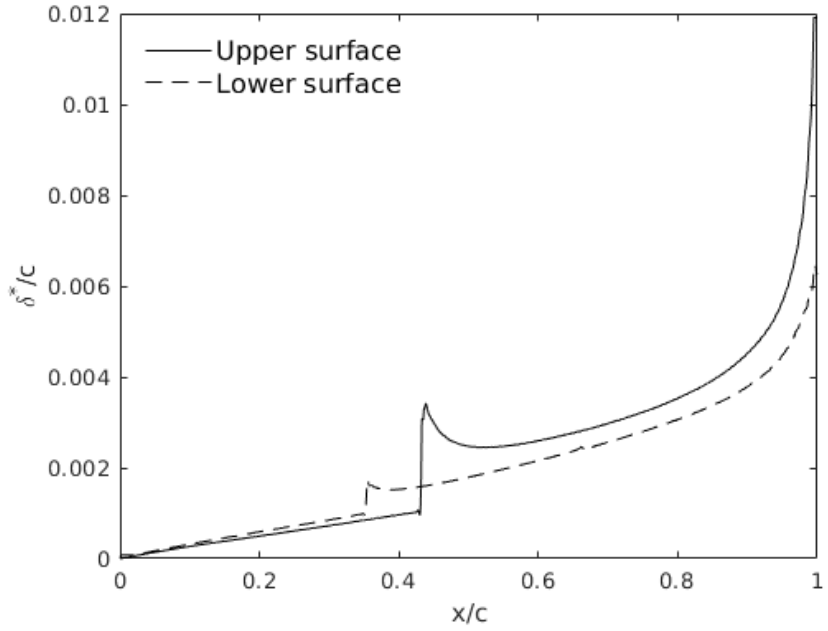

Figure 2 – Thickness of displacement for the NACA 0012 M = 0.750, $\alpha = 1.00^o$

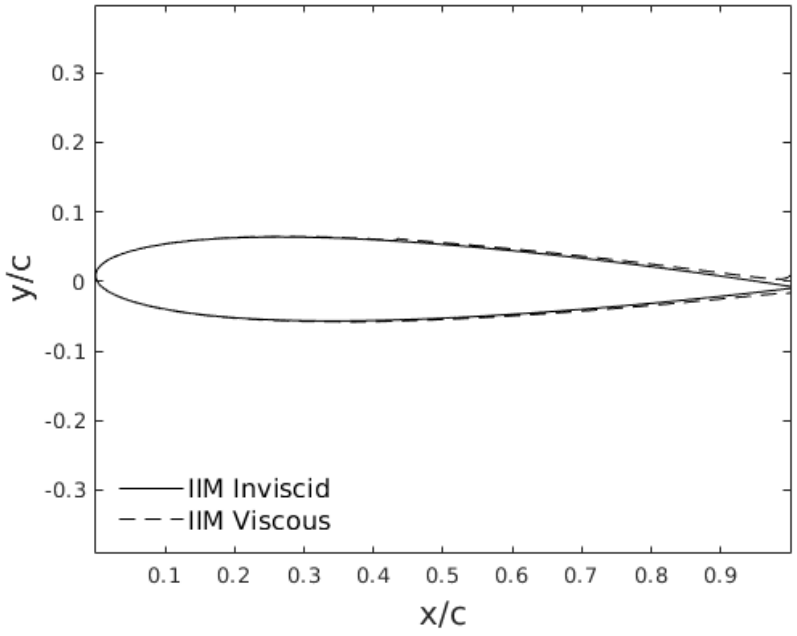

Figure 3 – Alteration in the shape of the airfoil NACA 0012 M = 0. 750, $\alpha = 1.00^o$ for the viscous correction

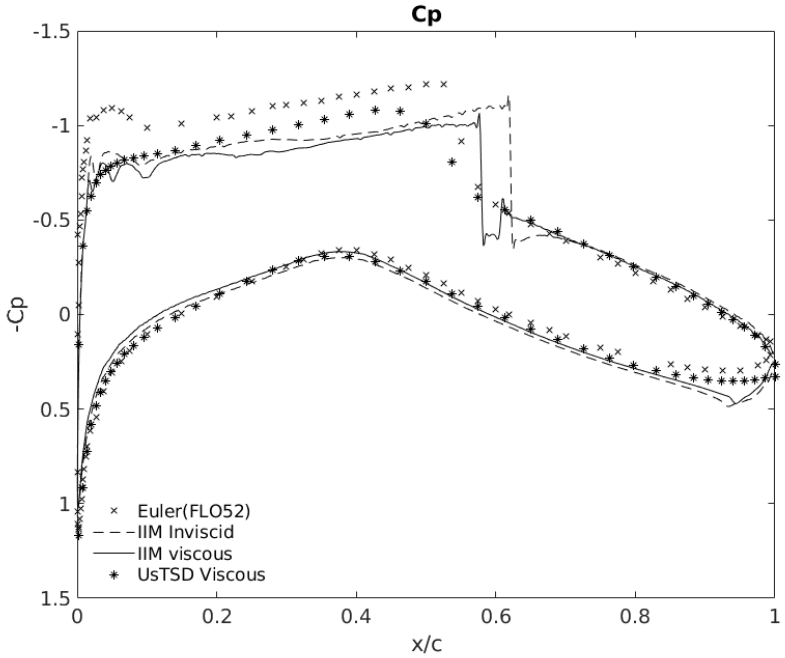

Figure 4 – Pressure coefficient for the RAE 2822 airfoil with Mach=0.729, $\alpha = 2.31^o$, with and without viscous correction.

case; and although it is small compared to the thickness of the original aerodynamic profile, it is not evident how much the thickening of δ^* is even in figure 2. Likewise, viscous effects cause the geometry of the profile to change.

4. RAE 2822

The viscous correction method was applied to the aerodynamic profile RAE 2822, this profile is designed for drag reduction. Two cases of close Machbut with different angles of attack are presented, the mesh was worked with 1380 nodes in the geometry, 1100, nodes in the ns grid, 917 points in the x direction, and 310 in the y direction. , 0.0015 the minimum spacing ratio, 0.5533 the $\Delta x_{max}/c$ (maximum spacing in the x direction), 0.2881 the $\Delta y_{max}/c$ (maximum spacing in the x direction) with respect to profile chord. The results are compared with the experimental data of the report AGARD138 and also verified with the results of viscous correction applied to a TSD method.
As in the case of NACA 0012, the graphs are represented as follows: the figures present the pressure coefficient of the undefined results of the IIM denoted with the dotted line, Cp data after viscous correction shown with the consecutive line, experimental data shown with the x-shaped dotted line and finally Cp data from TSD method with $*$ dotted line viscose correction. Limit litter δ^* graphs with a dotted line as lower surface and consecutive line thickness in upper surface and geometry alteration graphs due to thickness generation δ^* also the pressure field and Mach number fields are presented for all the cases comparing shock waves with and without viscous correction.

4.1 Mach=0.729, $\alpha = 2.31^o$

In all the cases that were analyzed, a positive response was observed towards the implementation of the viscous co-direction code in the IIM embedded interface method code developed in the thesis SOLARTE and compared, the cases from two to five with the data of the work of citeGreco2016 which were developed with the method of UsTSD. Where it was observed that even though the shock wave is marked and strong in the cases made with the IIM method, In doing the correction, they are remarkably close to the experimental data made in the wind tunnel and soften more in the lower surface as the experimental data appear in most cases.
The thickness of the litter limit that is observed in the figures of δ^* is due to the separation of flow in the profile, it is also observed that where there is a pressure drop near the upper surface increases

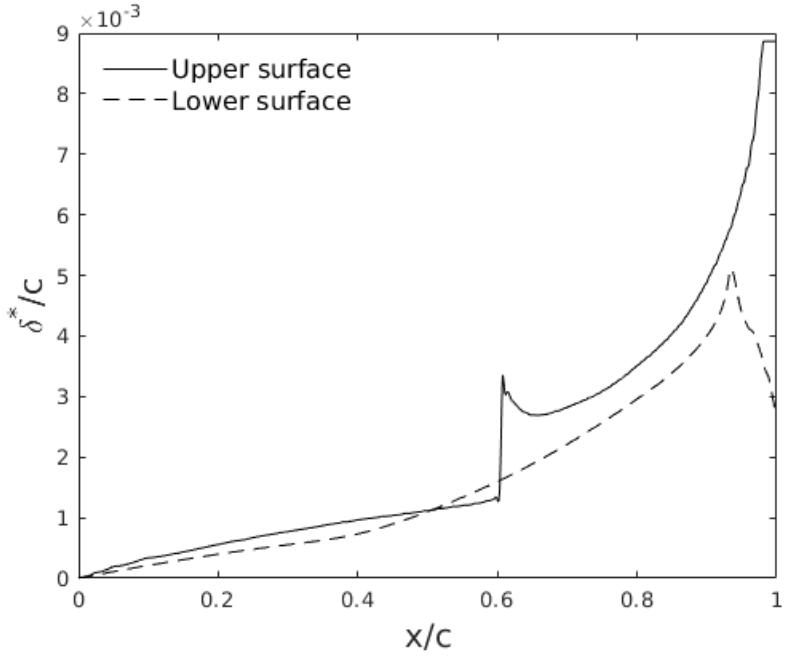

Figure 5 – Thickness of displacement for the RAE 2822 Mach=0.729, $\alpha = 2.31^o$

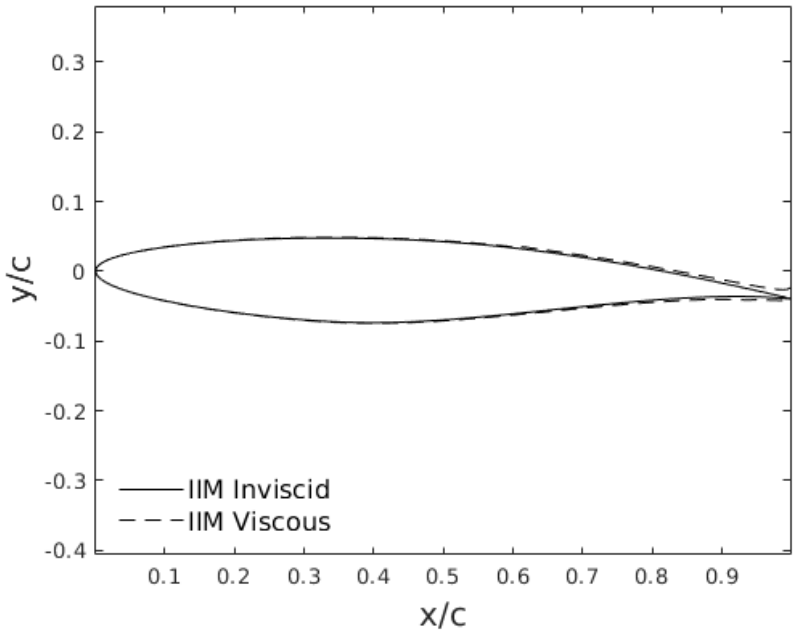

Figure 6 – Alteration in the shape of the aerofoil RAE 2822 Mach=0.729, $\alpha = 2.31^o$ for the viscous correction

the thickness of offshoring. In the graphs of pressure and speed in the inviscid and viscous cases as in the case of the profile NACA 0012 with Mach=0.750, $\alpha = 1.00^o$ is seen the approach of the shock wave in the upper surface towards the leading edge and the lower surface of shock is softened, as in the case of the NACA 0012 profile with Mach=0.750, $\alpha = 3.00^o$, with the difference that the shock wave in the lower surface continues to appear strong. In the profile NACA 0012 with Mach=0.800, $\alpha = 1.25^o$ the shock waves on the two surfaces approach with the correction to the leading edge and have a reduction in their strength in the lower surfaceas in experimental cases.
For the profile of RAE 2822 with Mach=0.729, $\alpha = 2.31^o$ and Mach = 0.730, $\alpha = 3.19^o$ the shock wave also moves towards the vanishing edge although without as much intensity as in the profile NACA 0012, and in the lower surface no sudden shock wave was generated in the undetected case.

5. Conclusions

The developed code corrects the viscosity in a compressible flow analysis work with the method of Immersed Interface between a solid surface and a fluid with the method of compact finite differences of the high order of precision in the special integration and Runge method High-order precision Kutta for the temporary integration of the aerodynamic profile NACA 0012 and RAE 2822, these results improved the deficiencies they had by not having a limit layer due to lack of viscosity.
The position of the shock wave was slightly different from the experimental results, although the softness of the shock wave was not improved on the upper surface, only on the lower in the cases presented. The convergence of the viscose correction calculations occurred in approximately five iterations. The results meet the objectives of this work.

6. Copyright Statement

References

[1] ADIBA et al. *eavy quark transport coefficients in a viscous qcd medium with collisional and radiative processes*. Physical Review D, 2021.

[2] AGARD *Experimental data base for computer program assessment*, 1979.

[3] ALLWRIGHT, E.; FORBES, L.; WALTERS, S.*Axisymmetric plumes in viscous fluids*.

[4] The ANZIAM Journal, v. 61, p. 1–29, 05 2019.

[5] ALOIS. An explanation and understanding of aerodynamic lift by triple deck theory. 11 2021.

[6] ANDERSON, J. D.; HUNTER, L. P. Introduction to Flight . [S.l.: s.n.], 1987. v. 40. 125–126 p. ISSN 0031-9228. ISBN 9780073380247.

[7] ANDERSON, J. D. J. John D. Anderson - Fundamentals of Aerodynamics,Third Edition (2001).pdf. 2001. 912 p.

[8] ASNAGHI, A.; SVENNBERG, U.; BENSOW, R. E. Evaluation of curvature correction methods for tip vortex prediction in SST k turbulence model framework. International Journal of Heat and Fluid Flow, v. 75, p. 135–152, 2019. ISSN 0142-727X.

[9] AWASKTHI, M. Viscous potential flow analysis of magnetohydrodynamic Rayleigh–Taylor instability with heat and mass transfer. International Journal of Dynamics and Control, v. 2, p. 254–261, 2013.

[10] AWASTHI, M.; ASTHANA, R.; AGRAWAL, G. Viscous corrections for the potential flow analysis of magneto-hydrodynamic kelvin-helmholtz instability with heat and mass transfer. The European Physical Journal A, v. 48, 11 2012.

[11] AWASTHI, M.; TAMSIR, M. Viscous corrections for the viscous potential flowanalysis of magnetohydrodynamic kelvin-helmholtz instability through porous media. Journal of Porous Media, v. 16, p. 663–676, 01 20013.

[12] AWASTHI, M. K. Viscous Corrections for the Viscous Potential Flow Analysis of Rayleigh–Taylor Instability With Heat and Mass Transfer. Journal of Heat Transfer, v. 135, n. 7, 2013. ISSN 0022-1481. Disponível em: <https://doi.org/10.1115/1.4023580>.

[13] AWASTHI, M. K.; ASTHANA, R.; AGRAWAL, G. S. Viscous correction for the viscous potential flow analysis of capillary instability with heat and mass transfer. Journal of Engineering Mathematics, v. 80, n. 1, p. 75–89, 2013. ISSN 1573-2703. Disponível em: <https://doi.org/10.1007/s10665-012-9597-2>. . Viscous correction for the viscous potential flow analysis of Kelvin-Helmholtz instability of cylindrical flow with heat and mass transfer. International Journal of Heat and Mass Transfer, Elsevier Ltd, v. 78, p. 251–259, 2014. ISSN 00179310. Disponível em: <http://dx.doi.org/10.1016/j.ijheatmasstransfer.2014.06.082>. 66 Bibliography . Viscous correction for the viscous potential flow analysis of Kelvin–Helmholtz instability of cylindrical flow with heat and mass transfer. International Journal of Heat and Mass Transfer, v. 78, p. 251–259, 2014. ISSN 0017-9310. Disponível em: <http://www.sciencedirect.com/science/article/pii/S0017931014005547>.

[14] BALBEER; MISHRA, H. Heavy quark transport in a viscous semi-qgp. Physical Review D, v. 101, 03 2020.

[15] BASU. Viscous corrections on wings in incompressible flow. The Aeronautical Journal (1968), Cambridge University Press, v. 94, n. 932, p. 67–72, 1990.

[16] BEAM, R. M.; WARMING, R. F. An implicit finite-difference algorithm for hyperbolic systems in conservation-law form. Journal of Computational Physics, v. 22, n. 1, p. 87–110, 1976. ISSN 0021-9991. Disponível em: <http: //www.sciencedirect.com/science/article/pii/0021999176901108>.

[17] BHADURY, S. et al. First order dissipative hydrodynamics and viscous corrections to the entropy four-current from an effective covariant kinetic theory. Journal of Physics G: Nuclear and Particle Physics, v. 47, 05 2020.

[18] BHINDER, M.; MURPHY, J. Evaluation of the viscous drag for a domed cylindrical moored wave energy converter. Journal of Marine Science and Engineering, v. 7, p. 120, 04 2019.

[19] BRULL, S.; MéHATS, F. Derivation of viscous correction terms for the isothermal quantum euler model. ZAMM Journal of applied mathematics and mechanics: Zeitschrift für angewandte Mathematik und Mechanik, v. 90, p. 219–230, 03 2010.

[20] BRUUS, H.; SETTNES, M. Theory of viscous corrections to the acoustic radiation force on a suspended microparticle in a standing ultrasound wave. p. 18006–, 11 2011.

[21] CARLOS; REZAEI, A. S.; TAHA, H. Viscous extension of vortex methods for unsteady aerodynamics. Physics of Fluids, v. 33, p. 103606, 10 2021.

[22] CHENG, L. et al. A semi-implicit immersed boundary method for simulating viscous flow-induced sound with moving boundaries. Computer Methods in Applied Mechanics and Engineering, v. 373, p. 113438, 2021. ISSN 0045-7825. Disponível em: <http://www.sciencedirect.com/science/article/pii/S004578252030623X>.

[23] CHUNG, T. J. Computational fluid dynamics, second edition. [S.l.: s.n.], 2010. v. 9780521769. 1–1034 p. ISBN 9780511780066.

[24] CRESCI. Compressible turbulent boundary layer with pressure gradient and heat transfer. AIAA Journal, v. 4, n. 1, p. 19–25, 1966. Disponível em: <https://doi.org/10.2514/3.3378>.

[25] DEREK. Viscous corrections to spectra, elliptic flow, and hbt radii. Nuclear Physics A, v. 715, 09 2002.

[26] DING, F. et al. Boundary-layer viscous correction method for hypersonic forebody/inlet integration. Acta Astronautica, v. 189, 09 2021. Bibliography 67

[27] DIPIN et al. A viscous potential flow model for core-annular flow. Applied Mathematical Modelling, v. 40, 12 2015.

[28] FUNADA , T. Pressure corrections for potential flow analysis of capillary instability of viscous fluids. Journal of Fluid Mechanics, v. 522, p. 383 – 394, 01 2005.

[29] GRECO Jr, P.; SHENG, L. A fast viscous correction method applied to small disturbance potential transonic flows in the frequency domain. In: . [S.l.: s.n.], 2004.

[30] GRECO, P. C. Contribuição ao estudo numérico da aerodinâmica em regime transônico. 2016.

[31] GU, N.; LU, Z.; GUO, T. Simulation of viscous flows around a moving airfoil by field velocity method with viscous flux correction. Advances in Applied Mathematics and Mechanics, v. 4, n. 3, p. 294–310, 2012. ISSN 20700733.

[32] GUIAS, R.; MITTAL, R.; DONG, H. A sharp interface immersed boundary method for compressible viscous flows. Journal of Computational Physics, v. 225, n. 1, p. 528–553, 2007. ISSN 0021-9991. Disponível em: <http://www.sciencedirect.com/science/ article/pii/S0021999106006048>.

[33] HAI-BAO et al. Electric and viscous correction for viscous potential flow analysis of electrohydrodynamic instability of an electrified leaky-dielectric jet. Physics of Fluids, v. 33, p. 114109, 11 2021.

[34] HAITHEM. Unsteady viscous lift frequency response using the triple deck theory. 01 2018.

[35] HALILA, G. L. O. et al. Efficient aerodynamic analysis for propeller aircraft including viscous effects. 12

2021. HERMAN. A differential turbomachinery equation with viscous correction. NASA

[36] STI/Recon Technical Report N, 07 1990. . Some implications of a differential turbomachinery equation with viscous correction. NASA STI/Recon Technical Report N, p. 25, 03 1993.

[37] HESSE, R. et al. Low global-warming-potential refrigerant CH2F2 (R-32): Integration of a radiation heat loss correction method to accurately determine experimental flame speed metrics. Proceedings of the Combustion Institute, 2020. ISSN 1540-7489. Disponível em: <http://www.sciencedirect.com/science/article/pii/S1540748920300444>.

[38] HIDEAKI et al. Viscous correction and shock reflection in stunted busemann intakes. In: . [S.l.: s.n.], 2018. p. 179–196. ISBN 978-3-319-73179-7. HOLST, T. L. Transonic flow computations using nonlinear potential methods. Progress in Aerospace Sciences, v. 36, n. 1, p. 1–61, 2000. ISSN 0376-0421. Disponível em: <http://www.sciencedirect.com/science/article/pii/S037604219900010X>.

[39] HU, S. et al. Zonal disturbance region update method for steady compressible viscous flows. Computer Physics Communications, v. 244, p. 97–116, 2019. ISSN 0010-4655. Disponível em: <http://www.sciencedirect.com/science/article/pii/S0010465519302024>.

[40] HUAN, J.; HUANG, T. Surface ship total resistance prediction based on a nonlinear free surface potential flow solver and a reynolds-averaged navier-stokes viscous correction. Journal of Ship Research, v. 51, p. 47–64, 03 2007. 68 Bibliography

[41] J.; NAKWACKI, M. Thermal photon production in au+au collisions: Viscous corrections in two different hydrodynamic formalisms. Nuclear Physics A, v. 851, p. 44–57, 10 2010.

[42] JIDE; QI, C. Longitudinal motion prediction of hybrid monohull considering three-dimensional viscous correction. p. 81–, 10 2011.

[43] JONATHAN. High order immersed interface method for compressible transonic flows. 2019, 2019.

[44] JOSEPH, D.; WANG, J. Viscous pressure correction in the irrotational flow outside prandtl's boundary layer. -1, 10 2004.

[45] JOSEPH, D. D.; FUNADA, T. Viscous contributions to the pressure for potential flow analysis of capillary instability of two viscous fluids. Physics of Fluids, v. 17, n. 5, p. 52105, 2005. Disponível em: <https://doi.org/10.1063/1.1914573>.

[46] JOSEPH , D.; WANG, J. The dissipation approximation and viscous potential flow. Journal of Fluid Mechanics, v. 505, p. 365 – 377, 04 2004.

[47] KARIM; VERZICCO, R.; ORLANDI, P. A numerical study of three-dimensional vortex ring instabilities: Viscous corrections and early nonlinear stage. Journal of Fluid Mechanics, v. 279, n. 5, p. 351–375, 1994. ISSN 14697645.

[48] KENNEDY, J.; MARSDEN, D. Viscous correction for wedge shaped impact probes.

[49] CASI Transactions, 03 1974.

[50] LATA; HIRONO, Y.; HAQUE, N. Quarkonium in a bulk viscous QGP medium. 2022.

[51] LEE. Computational Methods in Toxicoepigenomics. Toxicology and Epigenetics, p. 589–593, 2012.

[52] LEE, S.; THOMAS, S.; HOLST, T. Fast viscous correction method for full-potential transonic wing analysis. Journal of Aircraft, v. 24, 02 1984.

[53] LI, J.-D.; ZHAO, X.-D. Motion prediction of hybrid monohull considering viscous and bow up state effect. v. 13, p. 177–183, 04 2009.

[54] LIKUN; MARSTON, P. Acoustic radiation torque on small objects in viscous fluids and connection with viscous dissipation. The Journal of the Acoustical Society of America, v. 136, p. 2917, 12 2014.

[55] LIU, W. et al. Local piston theory with viscous correction and its application. AIAA Journal, v. 55, p. 942–954, 2017. M, L.; WOLFF, J. M.; FLEETER, S. Locally analytical prediction of the viscous aerodynamics of an oscillating flat plate airfoil. Mathematical and Computer Modelling, v. 12, n. 6, p. 707–719, 1989. ISSN 0895-7177. Disponível em: <http://www.sciencedirect.com/science/article/pii/0895717789903567>.

[56] MÜLLER, U. R.; HENKE, H. Computation of subsonic viscous and transonic viscous- inviscid unsteady flow. Computers Fluids, v. 22, n. 4, p. 649–661, 1993. ISSN 0045-7930. Disponível em: <http://www.sciencedirect.com/science/article/pii/004579309390030D>. Bibliography 69

[57] RAMANATHAN. International journal of research in aeronautical and mechanical engineering numerical scheme for 2-dimension optimum length nozzle contour design imposing viscous correction to method of characteristics. International Journal of Research in Aeronautical and Mechanical Engineering, v. 35, p. 10–17, 05 2015.

[58] SHANG. A new two-level defect-correction method for the steady Navier–Stokes equations. Journal of Computational and Applied Mathematics, Elsevier B.V., v. 381, n. 11361016, p. 113009, 2020. ISSN 03770427. Disponível em: <https://doi.org/10.1016/j.cam.2020.113009>.

[59] SMART, M. K. Design of Three-Dimensional Hypersonic Inlets with Rectangular-to- Elliptical Shape Transition. Journal of Propulsion and Power, v. 15, n. 3, p. 408–416, 1999. Disponível em: <https://doi.org/10.2514/2.5459>.

[60] TEREVIN. 1i Rki". Disponível em: <https://apps.dtic.mil/dtic/tr/fulltext/u2/238292. pdf>.